DE GRUYTER OPEN

*Journal of* ELECTRICAL ENGINEERING, VOL. 66, NO. 1, 2015, 26–33

# MULTI–FREQUENCY ANALYSIS FOR INTERSTITIAL MICROWAVE HYPERTHERMIA USING MULTI–SLOT COAXIAL ANTENNA

**Piotr Gas** *

The presented paper shows a new concept of multi-slot coaxial antenna working at different frequencies to predict the best solution for interstitial microwave hyperthermia treatment. The described method concerns a microwave heating of unhealthy cells using a thin microwave antenna located in the human tissue. Therefore, the coupled wave equation in a sinusoidal steady-state and the transient bioheat equation under an axial symmetrical model are considered. The 4-Cole-Cole approximation has been used to compute the complex relative permittivity of the human tissues at different antenna operating frequencies. At the stage of numerical simulation the finite element method (FEM) is used. Special attention has been paid to estimate the optimal antenna parameters for thermal therapy for three microwave frequencies mainly used in medical practice and make comparison of the obtained results in the case of single-, double- and triple-slot antennas.

K e y w o r d s: interstitial microwave hyperthermia, multi-slot coaxial antenna, cancer treatment, FEM, simulation

## 1 INTRODUCTION

Hyperthermia, besides radiotherapy and chemotherapy, plays an important role in modern oncology [1]. The phenomenon of this treatment is based on thermal sensitivity changes of living cells. In the specific therapeutic range of temperatures from 40 °C to 45 °C normal cells remain intact while the pathological ones are destroyed by the growing influence of necrosis and apoptosis [2]. When the temperature of 45 °C will be exceeded it may cause irreversible changes within normal and malignant tissues, including denaturation of proteins and tissue coagulation. This phenomenon is exploited by so-called thermoablation [3]. Therefore, a very important problem in hyperthermia treatment is to predict and precisely control the temperature in the target area to minimize the possibility of overheating and damaging healthy tissues. A lot of papers have examined different types of interstitial applicators for microwave heating purpose including the floating sleeve dipole, triaxial, choke, and cap-choke antennas [4]. Antennas fed with coaxial cable are very popular in thermal therapy because of their simple construction, small dimensions and low costs of production [5]. Until now, the coaxial-slot antennas have been described in many scientific and medical papers, but most of them have included only one [6, 7, 24] or two air gaps [8, 9]. It should be noted that the first publication, where the microwave heating using a new triple-slot coaxial antenna has been proposed, was published in 2014 [10]. What is important, the interstitial microwave hyperthermia treatment delivers energy directly to the place of interest using a coaxial-slot antenna invasively inserted into the tissue. This technique can be successfully applicable to a deep-seated tumor. Depending on the amount of delivered power and the antenna working frequency, microwaves heat up the tissue and induce thermal lesions in the distance up to 6 cm from the needle applicator [11]. Moreover, type of tumor, its location and severity, as well as the level of therapeutic temperature affect on the duration of single hyperthermia session, which can be maintained average for 40-60 min. Also it has been proved that temperatures above 42 °C can increase the sensitivity of cancerous cells treatment comparing to radio- and chemotherapy [12].

There are currently three ISM (industrial, scientific and medical) bands dedicated for microwave heating of tissues used by medical devices, namely 433.05–434.79 MHz utilized in Europe, 902–928 MHz applicable in the USA and 2400–2500 MHz available worldwide [13]. What is important, they are periodically verified by the International Telecommunication Union (ITU) based in Geneva. Therefore, frequencies of 434 MHz (wavelength 69 cm), 915 MHz (wavelength 33 cm) and 2450 MHz (wavelength 12 cm) are the most widely used in medical practice of hyperthermia treatment [7]. For this reason, the above mentioned frequencies have been examined in this paper. It should be emphasized that at the moment also the high-frequency systems for microwave heating purposes using frequencies up to 18 GHz have been successfully tested [4]. Higher frequencies can lead to design new interstitial devices with smaller dimensions and less invasiveness. Parallel with microwave hyperthermia techniques the utilization of magnetic nanoparticles for cancer treatment has been extensively examined [3, 14, 23].

This paper is dedicated to the multi-frequency analysis of single-, double- and triple-slot coaxial antennas, used in the interstitial microwave hyperthermia treatment. The content of the following article is the continuation of the study published earlier [10]. Special attention has been paid to estimate of the main elevations of antenna input

* AGH University of Science and Technology, al. Mickiewicza 30, 30-059 Krakow, Poland, piotr.gas@agh.edu.pl

DOI: 10.1515/jee-2015-0004, Print ISSN 1335-3632, On-line ISSN 1339-309X 

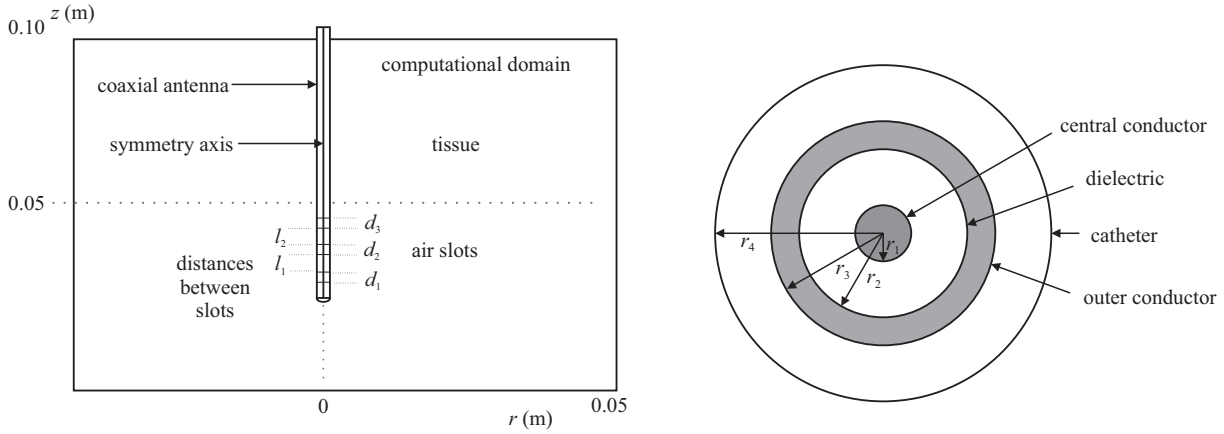


**Fig. 1.** Model of the multi-slot coaxial antenna including the dimensions, air gap configurations and the internal antenna structure

power for optimal thermal therapy separately for each of the air gap configurations. This will result in maintaining the temperature of the heated tissue exactly in the range of 40–45 °C and allow obtaining more comparable simulation results. The comparative analysis for multi-slot coaxial antennas with three microwave frequencies typically used in medical practice and commonly treated tissues is unique topic in modern hyperthermia therapy.

## 2 MODEL DEFINITION AND BASIC EQUATIONS

The two-dimensional axisymmetric model of the multi-slot microwave antenna is shown in Fig. 1. Described coaxial antenna is composed of such elements as central conductor, dielectric, outer conductor and a plastic catheter that protect the inner elements. Antenna dimensions examined in this paper are the same as in [9, 10]. What is more, the microwave needle applicator has three air slots of equal length $d_1 = d_2 = d_3 = 1\,\text{mm}$ positioned in the outer conductor at the $z_1 = 36.0\,\text{mm}$, $z_2 = 40.2\,\text{mm}$ and $z_3 = 44.4\,\text{mm}$. The distances between the gaps have the same values, namely $l_1 = l_2 = 4.2\,\text{mm}$.

The main simplifying assumption in presented simulation is that the human tissue and the microwave antenna are considered as uniform, linear and isotropic media. In the presented model the wave equation can be solved with respect to the complex vector of the magnetic field strength $\mathbf{H}$, as

$$\nabla \times \left[\underline{\varepsilon}_r^{-1} \nabla \times \mathbf{H}\right] - \omega^2 \varepsilon_0 \mu_0 \mu_r \mathbf{H} = 0 \tag{1}$$

where $\varepsilon_0$ means the electric constant equal to $8.854 \times 10^{-12}\,(\text{F m}^{-1})$ and $\mu_0$ —- the magnetic constant equal to $4\pi \times 10^{-7}(\text{H m}^{-1})$. Additionally, $\varepsilon_r$ and $\mu_r$ are the relative permittivity and permeability, respectively, $\omega$ denotes the electromagnetic field pulsation and $j = \sqrt{(-1)}$ is the imaginary unit.

In the above equation $\underline{\varepsilon}_r = \varepsilon_r' - j\varepsilon_r''$ is the frequency-dependent complex relative permittivity. What is important, the imaginary part of complex permittivity $\varepsilon_r''$ is associated with the energy dissipation. Therefore it is called the dielectric loss factor and determines the energy losses due to the phenomenon of dielectric polarization. In human tissues $\underline{\varepsilon}_r$ can be approximated by the 4-Cole-Cole model derived from measurements conducted by Camelia Gabriel and Sami Gabriel [15], that best fits the four dispersion regions $(\alpha, \beta, \delta, \gamma)$ occurring in living tissues

$$\underline{\varepsilon}_r(\omega) = \varepsilon_\infty + \sum_{n=1}^{4} \frac{\Delta\varepsilon_n}{1 + (j\omega\tau_n)^{1-\alpha_n}} - j\frac{\sigma_s}{\omega\varepsilon_0} \tag{2}$$

where $n$ is the number of independent dielectric relaxation processes with dielectric increments $\Delta\varepsilon_n$, whose sum gives $\Delta\varepsilon = \varepsilon_s - \varepsilon_\infty$, which is measure of the relaxation process intensity. It is worth knowing, that $\varepsilon_\infty$ means the infinite limit of relative permittivity (*ie* when $\omega\tau \gg 1$), $\varepsilon_s$ — the static limit of relative permittivity (*ie* when $\omega\tau \ll 1$), $\tau$ — the relaxation time constant (s) and $\sigma_s$ — the static conductivity of the material $(\text{Sm}^{-1})$. What is more, $\alpha$ is so-called the Cole-Cole parameter which is measure of broadening of the relaxation times in biological media [16]. Therefore, this parameter is determined by the distribution of relaxation times. Theoretically, it takes values between $0 \leq \alpha \leq 1$, but for the most biological substances it does not exceed the value of 0.5 (see Table. 1). It should be stressed that, the 4-Cole-Cole model provide the appropriate data for spectrum extending from 10 Hz to 100 GHz.

Due to the axial symmetry of multi-slot antenna, the presented model uses cylindrical coordinates $(r, \phi, z)$ with the transverse magnetic (TM) waves. For this reason, the magnetic field $\mathbf{H}$ has only a tangential component and the electric field $\mathbf{E}$ propagates in the $r$–$z$ plane. Therefore, $\mathbf{H} = H_\phi \mathbf{e}_\phi$, and $\mathbf{E} = E_r \mathbf{e}_r + E_z \mathbf{e}_z$, and equation (1) simplifies to the following scalar form

$$\nabla \times \left[\underline{\varepsilon}_r^{-1} \nabla \times H_\phi\right] - \omega^2 \varepsilon_0 \mu_0 \mu_r H_\phi = 0\,. \tag{3}$$

One of the basic thermal models that describe the heat flow inside the biological systems is so-called bioheat equation defined by Harry H. Pennes based on the classical Fourier law of heat conduction [17]. In the general

**Table 1.** Fitting parameters for the 4-Cole-Cole equation [15, 19]

| Tissue | $\varepsilon_\infty$ | $\Delta\varepsilon_n$ | | | | $\tau_n$ | | | | $\alpha_n$ | | | | $\sigma_s$ |
|---|---|---|---|---|---|---|---|---|---|---|---|---|---|---|
| | | 1 | 2 | 3 | 4 | 1 (ps) | 2 (ns) | 3 ($\mu$s) | 4 (ms) | 1 | 2 | 3 | 4 | (S/m) |
| brain | 4.0 | 40 | 700 | $20\times10^4$ | $45\times10^6$ | 7.958 | 15.915 | 106.103 | 5.305 | 0.10 | 0.15 | 0.22 | 0 | 0.04 |
| breast | 4.0 | 55 | 2500 | $10\times10^4$ | $40\times10^6$ | 7.958 | 159.155 | 159.155 | 159.155 | 0.10 | 0.10 | 0.20 | 0 | 0.50 |
| kidney | 4.0 | 47 | 3500 | $25\times10^4$ | $30\times10^6$ | 7.958 | 198.944 | 79.577 | 4.547 | 0.10 | 0.22 | 0.22 | 0 | 0.05 |
| liver | 4.0 | 39 | 6000 | $5\times10^4$ | $30\times10^6$ | 8.842 | 530.516 | 22.736 | 15.915 | 0.10 | 0.20 | 0.20 | 0.05 | 0.02 |
| lung | 2.5 | 18 | 500 | $25\times10^4$ | $40\times10^6$ | 7.958 | 63.662 | 159.155 | 7.958 | 0.10 | 0.10 | 0.20 | 0 | 0.03 |

**Table 2.** Physical parameters for the Pennes equation [19, 20]

| Tissue | $\lambda$ | $\rho$ | $C$ | $F$ | $\omega_b$ | $Q_{\mathrm{met}}$ |
|---|---|---|---|---|---|---|
| | W/(m K) | kg m$^3$ | J/kg K | ml/min/kg | 1/s | W/m$^3$ |
| brain | 0.51 | 1046 | 3630 | 559 | 0.009475 | 10642 |
| breast | 0.33 | 1058 | 2960 | 150 | 0.002645 | 2537 |
| kidney | 0.53 | 1066 | 3763 | 3795 | 0.067425 | 19428 |
| liver | 0.52 | 1079 | 3540 | 860 | 0.015466 | 5301 |
| lung | 0.39 | 394 | 3886 | 401 | 0.002633 | 2647 |
| blood | 0.52 | 1050 | 3617 | – | – | – |

case for the transient analysis this equation is governed by

$$\rho C\frac{\partial T}{\partial t}+\nabla\cdot(-\lambda\nabla T)=\rho_b C_b\omega_b(T_b-T)+Q_{\mathrm{ext}}+Q_{\mathrm{met}} \quad (4)$$

where $T$ denotes the tissue temperature (K) and $t$ is the time (s). The first term of the above equation describes the phenomenon of heat accumulation during the time which is determined by parameters such as the tissue specific heat $C$ ($\mathrm{J\,kg^{-1}K^{-1}}$) and the tissue density $\rho$ ($\mathrm{kg\,m^{-3}}$). The second term relates to the phenomenon of heat conduction in the tissue, which is determined by the tissue thermal conductivity $\lambda$ ($\mathrm{W\,m^{-1}K^{-1}}$). The third term describes the heat exchange between the tissue and blood and specifies the heat losses caused by tissue blood flow (perfusion) [18]. What is important, the subscript "$b$" refers to the blood, such in $\omega_b$ which means the blood perfusion rate ($\mathrm{s^{-1}}$). The last two terms relate to the heat generation, and are defined by two volumetric power densities, so-called: the metabolic heat generation rate $Q_{\mathrm{met}}$ ($\mathrm{W\,m^{-3}}$) produced by cell metabolic processes and the external heat $Q_{\mathrm{ext}}$ ($\mathrm{W\,m^{-3}}$) produced by sources of electromagnetic field, in our case by the multi-slot coaxial microwave antenna.

In the field of hyperthermia, the blood flow often is expressed in specific units of ml/min/kg, therefore to use it in equation (4) it is necessary to convert it into SI units according to the equation

$$\omega_b=\frac{1}{6}F\times10^{-7}\rho\left(\frac{1}{s}\right) \quad (5)$$

where $F$ is the blood flow rate in tissue (ml/min/kg).

Detailed derivation of the basic equations and specific description of the initial-boundary conditions on the presented model may be found in similar works [7,9–10].

The following analysis of the multi-slot coaxial antenna was made for three microwave working frequencies commonly used in medical practice, namely 434 MHz, 915 MHz and 2.45 GHz [7]. The dielectric parameters of the antenna elements have been taken from [9, 10]. The electro-thermal parameters of tissues have been retrieved from the IT'IS foundation materials database [19]. Table 1 contains fitting parameters appeared in the 4-Cole-Cole equation. Thermal properties are gathered together in Table 2. The values of the blood perfusion rate $\omega_b$ have been designated from the formula (5) and levels of the metabolic heat generation rate $Q_{\mathrm{met}}$ have been drawn on [20]. At the beginning of the heating, the tissue temperature has had initial value of $T_0 = 310.15\,\mathrm{K}$, which corresponds to the physiological temperature of the human body 37 °C. The blood temperature $T_b$ has been established on the same level.

The governing equations (3) and (4) with the appropriate initial-boundary conditions have been solved using the finite element method. All FEM computations have been performed using the Comsol Multiphysics software. The model for microwave cancer therapy with coaxial-slot antenna available in Comsol software developed by [6] and described in [21] has been adapted for the microwave heating using multi-slot coaxial antenna shown in this study. Moreover, the MATLAB environment has

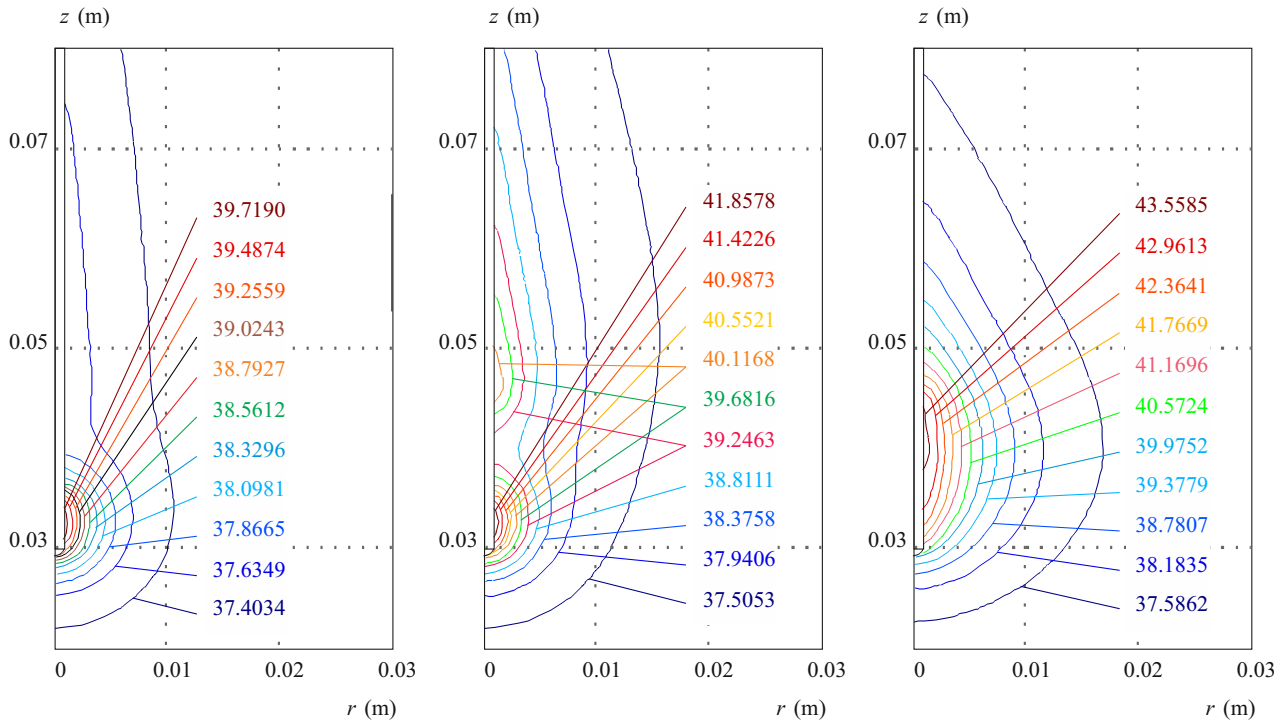


**Fig. 2.** Isotherms within the human brain tissue derived from the triple-slot coaxial microwave antenna for for various frequencies, namely: 434 MHz (left), 915 MHz (center) and 2450 MHz (right) and the total antenna input power set at $P_{\text{in}} = 2$ W in the steady-state

been used to present the simulation results. What is interesting, the Comsol's model is well known in the scientific world and it has been validated with a large number of numerical experiments and measurements [6, 9]. However, it should be pointed that the multi-frequency analysis of the microwave antenna with different active slot configurations presented in this paper does not have equivalents in similar papers. The outline of article can be found in the conference proceedings [22].

## 3 SIMULATION RESULTS AND DISCUSSION

The first step in the presented simulation was to estimate the exact elevations of the antenna input power individually for each of the air gap configurations such that the goal temperature in the targeted area does not exceed values of 40–45 °C. In this way, optimum conditions for the hyperthermia treatment are being obtained as indicated in the introduction. To do this, each of the analysed cases has been solved under $P_{\text{in}}$ arbitrarily assumed as 2 W. Sample contour plots of the temperature inside the human brain tissue under three basic microwave frequencies used in simulation are shown in Fig. 2. The presented plots demonstrate that the distributions of the isotherms are heterogeneous and local temperature maxima may occur in the computational area. The next step was to identify coordinates of the points at the interface between the antenna-tissue (on the surface of the catheter $r = r_4 = 0.895$ mm) characterized by the highest temperatures. These specific points $(r_4, z_m)$ have been provided in Table 3 and for them the further calculations have been made.

It should be emphasized that due to the different active slot configurations, the microwave antenna can produce a non-uniform temperature distribution inside the tissue. Therefore, on the path $r = 0.895$ mm can observe two temperature peaks of which the first $(^*)$ or second $(^{**})$ dominates as indicated in Table 3. What is important, they occur only for operating frequencies of 915 MHz and 2.45 GHz in the case of certain double- and triple-slot antennas. Moreover, the similar values of $z_m$ were obtained for the frequency of 434 MHz and 915 MHz. The small differences are due to numerical errors, different division of the computational area into the finite elements or choosing the temperature for a neighboring element node. For the frequency of 2.45 GHz the local temperature maxima move up the $z$ axis of approximately 4–10 mm. The next step was determining the parametric solution for the temperature distributions depending on the total antenna input power at all pre-selected points (see Fig. 3 left) and establishing specific limit values of the $P_{\text{in}}$ for optimal interstitial microwave hyperthermia treatment. All resulting data have been compared in Table 4 and utilized for subsequent simulations. Figure 3 (right) also shows the example of paired temperature distributions along predefined path to confirm that the therapeutic range of temperature 40–45 °C have not been exceeded.

The analysis of this table leads to the conclusion that the total input power decreases with increasing antenna working frequency and the smallest values of $P_{\text{in}}$ are required for heating of the breast tissue. For frequencies 434 MHz and 915 MHz slight power changes are observed

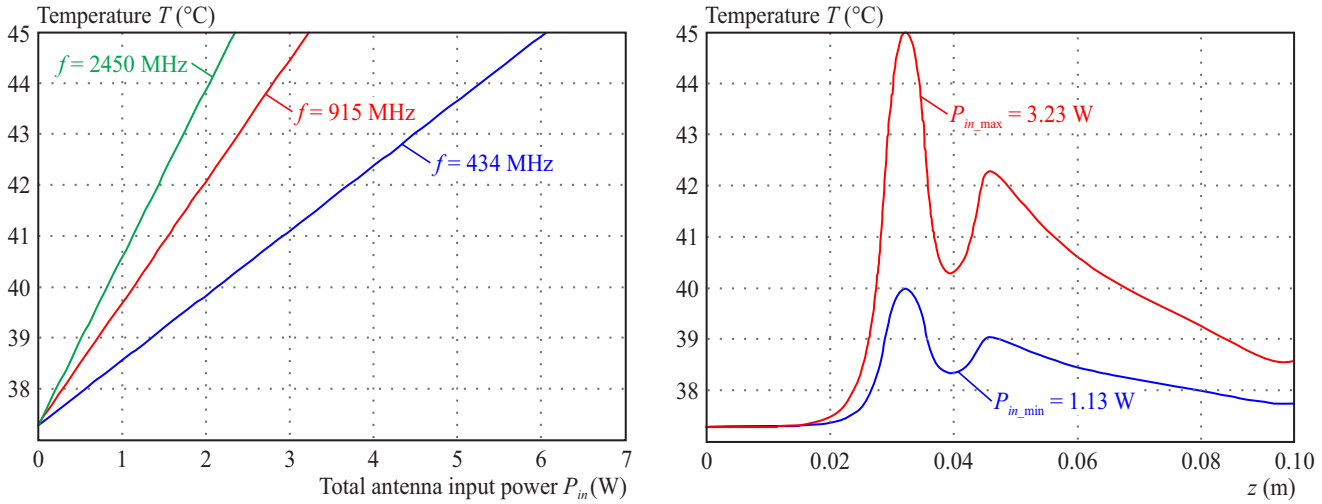


**Fig. 3.** Temperature versus the total antenna input power at the point where the highest temperature at the interface antenna-tissue has occurred (left) and temperature distributions along $r = 0.895$ mm in the brain tissue for $f = 915$ MHz and pre-set limit values of $P_{\text{in}}$ (right) obtained from the triple-slot antenna

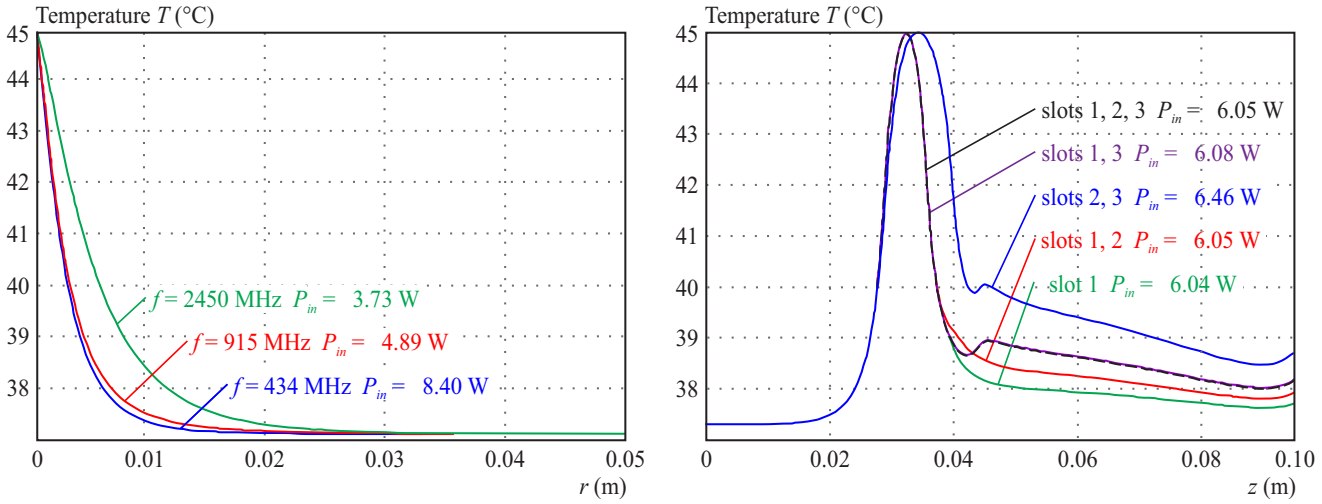


**Fig. 4.** Temperature distributions produced by the triple-slot antenna along the path $z = z_m$ for various frequencies (left) and temperature distributions along $r = 0.895$ mm for $f = 434$ MHz produced by the coaxial antennas with different active slots (right) for the brain tissue and $P_{\text{in max}}$ in the steady-state

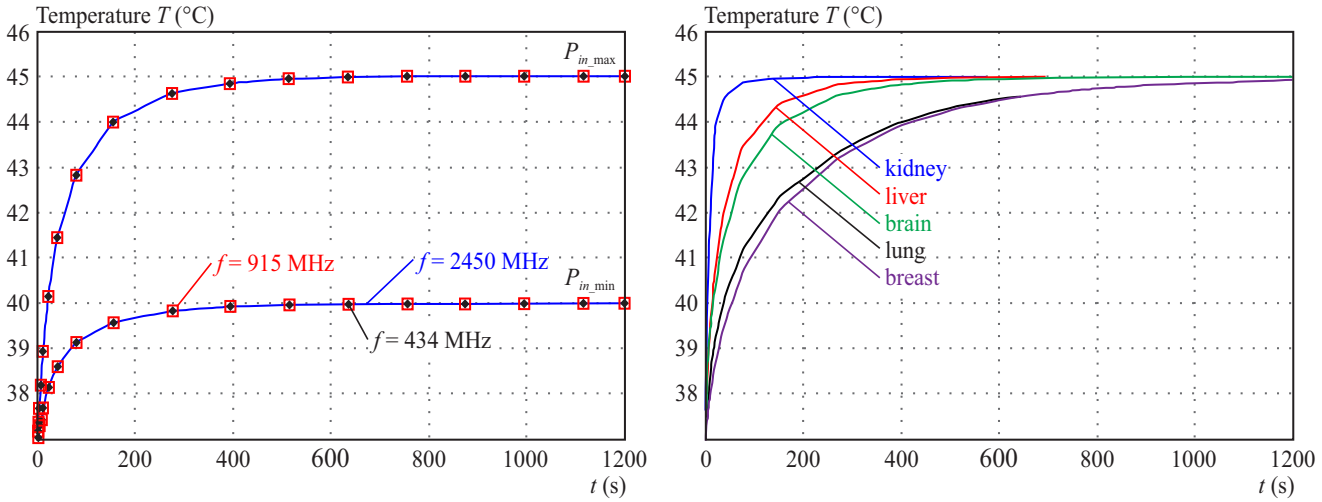


**Fig. 5.** Examples of transient temperature distributions at points $r = 0.895$ mm and $z = z_m$ for the triple-slot coaxial antennas within the breast tissue for different frequencies and limit values of $P_{\text{in}}$ (left) as well as for various tissues and $f = 2450$ MHz (right)

**Table 3.** The coordinates $z_m$ of the points with maximum temperature elevations along the path $r = 0.895$ mm in the steady-state ($z_m$ dimension is in mm)

| | | Number of active slot | | | | |
|---|---|---|---|---|---|---|
| Frequency | Tissue | 1 | 1, 2 | 1, 3 | 2, 3 | 1, 2, 3 |
| 434 MHz | brain | 32.66 | 32.66 | 32.66 | 34.67 | 32.66 |
| | breast | 32.66 | 32.66 | 32.66 | 34.67 | 32.66 |
| | kidney | 32.66 | 32.66 | 32.66 | 33.67 | 32.66 |
| | liver | 32.66 | 32.66 | 32.66 | 34.17 | 32.66 |
| | lung | 32.66 | 32.66 | 32.66 | 34.67 | 32.66 |
| 915 MHz | brain | 32.66 | 32.66* | 32.66* | 34.17* | 32.66* |
| | breast | 33.17 | 32.66* | 32.66* | 46.73** | 32.66* |
| | kidney | 32.66 | 32.16* | 32.16* | 33.17* | 32.16* |
| | liver | 32.66 | 32.16* | 32.16* | 33.67* | 32.16* |
| | lung | 32.66 | 32.66* | 32.16* | 33.67* | 32.16* |
| 2450 MHz | brain | 37.19 | 40.70 | 43.22 | 43.72 | 39.70 |
| | breast | 37.69 | 40.70 | 39.70 | 40.20 | 39.70 |
| | kidney | 36.68 | 40.70 | 43.72 | 44.22** | 39.70* |
| | liver | 37.19 | 40.70 | 43.72 | 44.22** | 40.20* |
| | lung | 37.19 | 41.21** | 44.22** | 44.72** | 44.72** |

*the first of the two temperature peaks is dominant,

**the second of two temperature peaks is dominant

within individual tissues (the smallest in lung tissue) and they are growing for antennas with the following slot configurations: 1, 1-2, 1-2-3, 1-3 as well as 2-3. In the case of frequency 2450 MHz the power changes are larger and the above sequence is changed as follows: 1, 1-2, 1-3, 1-2-3 and 2-3. In addition, the biggest antenna input powers (much greater from the other cases) are needed for the antenna with slots 2 and 3, especially for the kidney tissue. A further stage of the study was resolving each of the analysed cases for the ceiling levels of antenna input power $P_{\text{in max}}$. In this manner, the distributions for the maximum acceptable temperatures in the hyperthermia treatment have been obtained.

Figure 4 presents temperature variations along two different paths $z = z_m$ (left) and $r = 0.895$ mm (right) for the predefined values of $P_{\text{in max}}$ incorporating different frequencies and active air gaps of the multi-slot coaxial antenna. On these graphs, the therapeutic areas of heat operation in which the temperature is above 40 °C along each axis of the cylindrical coordinate system can be easily identified as detailed in Table 5.

It should be noted that the local temperature peaks experienced in distributions $T(z)$ have the same pattern as prescribed in the case of Table 3. For most of the analyzed cases, the right-side slope of the curve $T(z)$ remains the same, while its right-side slope is changed by extending and increasing its elevation. Furthermore, $\Delta_r$ increases with frequency and within the single frequency it changes in a similar sequence as the antenna input power $P_{\text{in}}$ mentioned earlier. The variations of $\Delta_z$ are arbitrary and do not take a particular pattern similar to $z_m$ values listed in Table 1. However, the therapeutic area has the largest size in the case of the antenna with slots 2 and 3 especially in the breast tissue for frequency 915 MHz. The smallest values of $\Delta_r$ and $\Delta_z$ exist in the kidney tissue for single-slot antenna working at frequency of 434 MHz.

At the end, the time dependencies of temperature at predefined points ($r = 0.895$ mm, $z_m$) and for pre-set values of the antenna input powers have been presented to show how heat accumulation occurs in the individual tissues depending on the frequency, see Fig. 5. The temperature reaches a steady-state most rapidly in the case of kidney tissue and the longest inside the breast tissue. Moreover, for a single frequency and within the same tissue the differences in the accumulation of heat are negligible.

## 4 CONCLUSIONS

The numerical simulations are usually more flexible and often more convenient to design new solutions in many modern technological problems. The approach presented in this paper offers a relatively simple methodology of finding the best model parameters for the optimal interstitial microwave hyperthermia treatment. Changing power delivered to the antenna in each analyzed case has allowed a better comparison of results than it took place in [10] where the antenna input power remained on the

**Table 4.** The limit values of antenna input power in (W) for optimal hyperthermia treatment

| Frequency | Tissue | Number of active slot | | | | | | | | | |
|---|---|---|---|---|---|---|---|---|---|---|---|
| | | 1 | | 1,2 | | 1,3 | | 2,3 | | 1,2,3 | |
| | | $P_{\text{in min}}$ | $P_{\text{in max}}$ | $P_{\text{in min}}$ | $P_{\text{in max}}$ | $P_{\text{in min}}$ | $P_{\text{in max}}$ | $P_{\text{in min}}$ | $P_{\text{in max}}$ | $P_{\text{in min}}$ | $P_{\text{in max}}$ |
| 434 MHz | brain | 2.12 | 6.04 | 2.13 | 6.05 | 2.14 | 6.08 | 2.27 | 6.46 | 2.13 | 6.05 |
| | breast | 1.40 | 3.93 | 1.40 | 3.94 | 1.41 | 3.97 | 1.42 | 4.00 | 1.40 | 3.95 |
| | kidney | 5.73 | 15.53 | 5.75 | 15.59 | 5.81 | 15.74 | 6.93 | 18.78 | 5.78 | 15.67 |
| | liver | 3.03 | 8.23 | 3.03 | 8.24 | 3.06 | 8.31 | 3.35 | 9.10 | 3.04 | 8.27 |
| | lung | 0.82 | 2.31 | 0.82 | 2.31 | 0.82 | 2.33 | 0.84 | 2.39 | 0.82 | 2.32 |
| 915 MHz | brain | 1.08 | 3.07 | 1.11 | 3.17 | 1.14 | 3.24 | 1.47 | 4.18 | 1.13 | 3.23 |
| | breast | 0.83 | 2.34 | 0.84 | 2.37 | 0.85 | 2.39 | 0.92 | 2.59 | 0.85 | 2.38 |
| | kidney | 3.03 | 8.22 | 3.11 | 8.41 | 3.17 | 8.60 | 4.61 | 12.50 | 3.15 | 8.53 |
| | liver | 1.69 | 4.60 | 1.74 | 4.74 | 1.78 | 4.84 | 2.37 | 6.43 | 1.77 | 4.81 |
| | lung | 0.48 | 1.36 | 0.50 | 1.42 | 0.52 | 1.47 | 0.63 | 1.79 | 0.52 | 1.46 |
| 2450 MHz | brain | 0.50 | 1.43 | 0.56 | 1.60 | 0.78 | 2.23 | 0.87 | 2.48 | 0.83 | 2.35 |
| | breast | 0.28 | 0.79 | 0.30 | 0.85 | 0.39 | 1.11 | 0.44 | 1.23 | 0.40 | 1.13 |
| | kidney | 1.42 | 3.84 | 1.60 | 4.33 | 2.33 | 6.32 | 2.62 | 7.11 | 2.51 | 6.79 |
| | liver | 0.79 | 2.14 | 0.88 | 2.39 | 1.22 | 3.32 | 1.37 | 3.73 | 1.34 | 3.63 |
| | lung | 0.34 | 0.96 | 0.41 | 1.16 | 0.55 | 1.55 | 0.61 | 1.73 | 0.59 | 1.68 |

**Table 5.** Therapeutic areas of heat operation along $r$ and $z$ axes ($\Delta_r, \Delta_z$ dimensions are in mm)

| Frequency | Tissue | Number of active slot | | | | | | | | | |
|---|---|---|---|---|---|---|---|---|---|---|---|
| | | 1 | | 1,2 | | 1,3 | | 2,3 | | 1,2,3 | |
| | | $\Delta_r$ | $\Delta_z$ | $\Delta_r$ | $\Delta_z$ | $\Delta_r$ | $\Delta_z$ | $\Delta_r$ | $\Delta_z$ | $\Delta_r$ | $\Delta_z$ |
| 434 MHz | brain | 4.05 | 9.90 | 4.12 | 9.90 | 4.14 | 9.70 | 4.72 | 14.70 | 4.14 | 9.70 |
| | breast | 4.65 | 10.90 | 4.76 | 11.30 | 4.81 | 11.10 | 5.61 | 26.00 | 4.80 | 11.10 |
| | kidney | 2.86 | 8.00 | 2.89 | 7.80 | 2.90 | 7.70 | 3.12 | 12.00 | 2.90 | 7.70 |
| | liver | 3.65 | 9.10 | 3.70 | 9.00 | 3.72 | 9.00 | 4.17 | 13.10 | 3.72 | 9.00 |
| | lung | 4.73 | 11.10 | 4.85 | 11.60 | 4.89 | 11.30 | 5.67 | 18.80 | 4.88 | 11.30 |
| 915 MHz | brain | 4.36 | 18.60 | 4.44 | 31.10∗ | 4.49 | 40.70* | 5.22 | 55.20* | 4.48 | 40.50* |
| | breast | 5.42 | 32.70 | 5.57 | 45.50∗ | 5.70 | 53.10* | 8.82 | 59.30** | 5.68 | 53.10* |
| | kidney | 2.97 | 10.50 | 2.98 | 20.30∗ | 3.00 | 28.30* | 3.27 | 47.90* | 3.00 | 28.10* |
| | liver | 3.86 | 13.50 | 3.88 | 24.10∗ | 3.91 | 33.30* | 4.48 | 51.60* | 3.91 | 33.10* |
| | lung | 4.99 | 14.50 | 5.01 | 21.60∗ | 5.10 | 32.10* | 5.96 | 50.60* | 5.09 | 31.80* |
| 2450 MHz | brain | 5.89 | 25.40 | 6.21 | 25.40 | 6.55 | 23.90 | 6.72 | 25.20 | 7.01 | 25.10 |
| | breast | 7.68 | 27.00 | 8.04 | 26.60 | 8.39 | 24.70 | 8.50 | 25.80 | 8.67 | 25.40 |
| | kidney | 3.74 | 20.90 | 3.87 | 21.10 | 3.97 | 20.90 | 3.98 | 21.70** | 4.47 | 21.70* |
| | liver | 5.27 | 24.50 | 5.54 | 24.40 | 5.70 | 22.80 | 5.74 | 24.20** | 6.41 | 24.40* |
| | lung | 6.99 | 32.00 | 7.69 | 33.70** | 7.87 | 30.60** | 7.93 | 32.10** | 8.12 | 33.50** |

*the first of the two temperature peaks is dominant,

**the second of two temperature peaks is dominant

same level within single frequency. The numerical simulations demonstrate that reducing the antenna operating frequency the level of total microwave power delivered to the antenna can be increased. Moreover, adding more air slots in the antenna structure also requires more input power to maintain the temperature at 45 °C. The simulation results suggest that for the triple-slot antennas, the quasi-uniform temperature distributions between gaps are observed, and the therapeutic area increases. In the case of the 2–3 slot antenna the therapeutic area of the heat penetration is even greater but temperature distribution is less homogeneous than other air gap config-

urations and local temperature maxima occur. Interestingly, the greatest heterogeneity occurs at the frequency of 915 MHz. It may affect on uneven heating of treated tissue. What is more, the elevations of the $P_{\text{in}}$ directly influence on the $\Delta_r$ changes and the position of temperature maximum $z_m$ has impact on variations of the $\Delta_z$. The temperature reaches a steady state in the slowest way for the breast tissue and the fastest for the kidney tissue. This all may have practical significance in finding new solutions for better cancer treatment. Using the appropriate antenna type and working frequency depends on the individual circumstances and should be taken into account what is planned to be exactly achieved in hyperthermia therapy.

## References


[1] ALLISON, R. R.: The Electromagnetic Spectrum: Current and Future Applications in Oncology, Future Oncology **9** No. 5 (2013), 657–667.

[2] GAS, P.: Essential Facts on the History of Hyperthermia and their Connections with Electromedicine, Przeglad Elektrotechniczny **87** No. 12b (2011), 37–40.

[3] HILGER, I.: In Vivo Applications of Magnetic Nanoparticle Hyperthermia, International Journal of Hyperthermia **29** No. 8 (2013), 828–834.

[4] LUYEN, H.—GAO, F.—HAGNESS, S. C.—BEHDAD, N.: Microwave Ablation at 10.0 GHz Achieves Comparable Ablation Zones to 1.9 GHz in Ex Vivo Bovine Liver, IEEE Transactions on Biomedical Engineering **61** No. 6 (2014), 1702–1710.

[5] ITO, K.—SAITO, K.: Development of Microwave Antennas for Thermal Therapy, Current Pharmaceutical Design **17** No. 22 (2011), 2360–2366.

[6] SAITO, K.—TANIGUCHI, T.—YOSHIMURA, H.—ITO, K.: Estimation of SAR Distribution of a Tip-Split Array Applicator for Microwave Coagulation Therapy Using the Finite Element Method, IEICE Transactions on Electronics **E84.C** No. 7 (2001), 948–954.

[7] GAS, P.: Tissue Temperature Distributions for Different Frequencies Derived from Interstitial Microwave Hyperthermia, Przeglad Elektrotechniczny **88** No. 12b (2012), 131–134.

[8] BRACE, C. L.: Dual-Slot Antennas for Microwave Tissue Heating: Parametric Design Analysis and Experimental Validation, Medical Physics **38** No. 7 (2011), 4232–4240.

[9] RATTANADECHO, P.—KEANGIN, P.: Numerical Study of Heat Transfer and Blood Flow in Two-Layered Porous Liver Tissue During Microwave Ablation Process using Single and Double Slot Antenna, International Journal of Heat and Mass Transfer **58** No. 1-2 (2013), 457–470.

[10] GAS, P.: Study on Interstitial Microwave Hyperthermia with Multi-Slot Coaxial Antenna, Revue Roumaine des Sciences Techniques-Serie Electrotechnique et Energetique **59** No. 2 (2014), 215–224.

[11] LOPRESTO, V.—PINTO, R.—CAVAGNARO, M.: Experimental Characterisation of the Thermal Lesion Induced by Microwave Ablation, International Journal of Hyperthermia **30** No. 2 (2014), 110–118.

[12] INMAN, B. A.—STAUFFER, P. R.—CRACIUNESCU, O. A.—MACCARINI, P. F.—DEWHIRST, M. W.—VUJASKOVIC, Z.: A Pilot Clinical Trial of Intravesical Mitomycin-C and External Deep Pelvic Hyperthermia for Non-Muscle-Invasive Bladder Cancer, International Journal of Hyperthermia **30** No. 3 (2014), 171–175.

[13] Report ITU-R SM.2180: Impact of Industrial, Scientific and Medical (ISM) Equipment on Radiocommunication Services, ITU, Geneva 2011.

[14] MIASKOWSKI, A.—SAWICKI, B.: Magnetic Fluid Hyperthermia Modeling based on Phantom Measurements and Realistic Breast Model, IEEE Transactions on Biomedical Engineering 60 No. 7 (2013), 1806–1813.

[15] GABRIEL, S.—LAU, R. W.—GABRIEL, C.: The Dielectric Properties of Biological Tissues: III. Parametric Models for the Dielectric Spectrum of Tissues, Physics in Medicine and Biology **41** No. 11 (1996), 2271–2293.

[16] GRIMNES, S.—MARTINSEN, O. G.: Alpha-Dispersion in Human Tissue, Journal of Physics: Conference Series **224** (2010), 1–4.

[17] PENNES, H. H.: Analysis of Tissue and Arterial Blood Temperatures in the Resting Human Forearm, Journal of Applied Physiology **85** No. 1 (1998), 5–34.

[18] HABASH, R. W. Y.—BANSAL, R.—KREWSKI, D.—ALHAFID, H. T.: Thermal Therapy, Part IV: Electromagnetic and Thermal Dosimetry, Critical Reviews in Biomedical Engineering **35** No. 1-2 (2007), 123–182.

[19] HASGALL, P. A.—NEUFELD, E.—GOSSELIN, M. C.—KLINGENBÖCK, A.—KUSTER, N.: IT'IS Database for Thermal and Electromagnetic Parameters of Biological Tissues, Version 2.5, August 1st 2014, available at: www.itis.ethz.ch/database.

[20] MCINTOSH, R. L.—ANDERSON, V.: Erratum: "A Comprehensive Tissue Properties Database Provided for the Thermal Assessment of a Human at Rest", Biophysical Reviews and Letters **8** No. 1 & 2 (2013), 99–100.

[21] PRYOR, R. W.: Multiphysics Modeling using Comsol: A First Principles Approach, Jones and Bartlett Publishers, 2011.

[22] GAS, P.: Transient Analysis of Interstitial Microwave Hyperthermia Using Multi-Slot Coaxial Antenna,, In GOŁEBIOWSKI, L.— MAZUR, D. (Eds.): Analysis and Simulation of Electrical and Computer Systems, Book series: Lecture Notes in Electrical Engineering, Vol. 324, (2015), Chapter 5, 63–71, Springer International Publishing, Switzerland.

[23] PARUCH, M.: Hyperthermia Process Control Induced by the Electric Field in order to Destroy Cancer, Acta of Bioengineering and Biomechanics **16** No. 4 (2014), 121–128.

[24] MOREGA, M.—MOREGA, A. M.—DIAZ, I. M.—SANDOIU, A. M.: Percutaneous Microwaves Hyperthermia Study by Numerical Simulation, In 2014 International Conference and Exposition on Electrical and Power Engineering (EPE), Iasi, Romania, 2014, pp. 498–503.


Received 15 June 2014

**Piotr Gas** is researcher of the Faculty of Electrical Engineering, Automatics, Computer Science and Biomedical Engineering at the AGH University of Science and Technology in Krakow, Poland. His interests concern the impact of electromagnetic fields on biological objects, biomedical and therapeutic applications of the electromagnetic fields and their standardization. His current work in the Department of Electrical and Power Engineering is focused on modelling of various phenomena of the electromagnetic hyperthermia.